Journal of Molecular Spectroscopy **210,** 41–50 (2001)
doi:10.1006/jmsp.2001.8442, available online at http://www.idealibrary.com on IDEAL®

The $X^2\Pi_i$, $A^2\Delta_i$, and $B^2\Sigma^+$ Low-Lying States of NiCl: Laser-Induced Fluorescence and Fourier Transform Emission Experiments

Y. Krouti,* A. Poclet,† T. Hirao,‡ B. Pinchemel,† and P. F. Bernath‡

Laboratoire de Physique Atomique et Moléculaire, Faculté des Sciences Aïn Chock, B.P. 5366 Maârif, Casablanca, Morocco; †Laboratoire de Physique des Lasers, Atomes et Molécules, UMR CNRS 8523 Centre d'Etudes et de Recherches Lasers et Applications, Université de Lille I 59655, Villeneuve d'Ascq Cedex, France; and ‡Department of Chemistry, University of Waterloo, Waterloo, Ontario, Canada N2L 3G1

Received April 17, 2001; in revised form September 5, 2001

Six new electronic transitions of NiCl, recorded by high-resolution Fourier transform spectroscopy, have been studied. The identification of the states involved in these transitions has been made possible by dispersing laser-induced fluorescence at low resolution. Comparison of the results obtained using these two experimental techniques allowed us to locate the [1.6] $A\,^2\Delta_{3/2}$ ($v = 0$) spin–orbit component at 1 646 cm^{-1} above the $X\,^2\Pi_{3/2}$ ground state. Two other low-lying states have also been identified: the first one, located 382 cm^{-1} above the ground state is a good candidate to be the $X\,^2\Pi_{1/2}$ component of the $X\,^2\Pi_i$ state. A second state at 1 385 cm^{-1} in the energy level diagram could be a component of a quartet state of NiCl. In addition we have identified a $\Omega = 3/2$ state 21 608 cm^{-1} above the $X\,^2\Pi_{3/2}$ ground state. The [22.3] $^2\Delta_{3/2}$ spin–orbit component associated with already known [21.9] $^2\Delta_{5/2}$ sublevel has also been identified.

I. INTRODUCTION

In two recent papers (*1, 2*) devoted to the analysis of the visible spectrum of NiCl, we demonstrated the complementarity of low-resolution laser-induced dispersed fluorescence experiments and Fourier transform spectroscopy. NiCl is similar to the isovalent molecule NiF (*3*), so three low-lying electronic states ($^2\Pi_i$, $^2\Delta_i$, and $^2\Sigma^+$) are expected in the first 2 000 cm^{-1} above the $X\,^2\Pi_{3/2}$ ground state. This causes an impressive number of intense (allowed) and weak (forbidden) transitions connecting to several upper electronic states. In addition, intervals between the electronic states are, in some cases, close to the values of the vibrational spacing. This can lead to mistakes in the identification of the electronic states linked by the observed transitions (*4*). Even when a rotational analysis is possible, it can happen that two close-lying states have almost equal rotational and fine structure constants, leading to erroneous identifications of the electronic states. It appears that the construction of a credible energy level diagram can be carried out by observation of dispersed laser-induced fluorescence. Such an energy level diagram is a useful starting point to study bands recorded at high resolution either by (time-consuming) laser excitation spectroscopy (*5*) or by (time-saving) Fourier transform spectroscopy (*1, 2*).

In this paper, we present the analysis of bands involving [1.6]$A\,^2\Delta_{3/2}$ spin–orbit component and the already known [24.9]$\,^2\Pi_{1/2}$, [24.5]$\,^2\Pi_{3/2}$, [21.9] $^2\Delta_{5/2}$ states as well as a new [21.6] $\Omega = 3/2$ electronic state. In addition a [22.3] $^2\Delta_{3/2}$ sublevel located at 22 362 cm^{-1} above the $X\,^2\Pi_{3/2}$ state can be associated with the already known [21.9]$\,^2\Delta_{5/2}$ spin–orbit component (*1*). We locate on the energy level diagram the [0.38]$\,^2\Pi_{1/2}$ state and an electronically unassigned low-lying state 1 385 cm^{-1} above the ground $X\,^2\Pi_{3/2}$ state.

II. EXPERIMENTAL DETAILS

Details about the experimental setups have been extensively described in Refs. (*1*) and (*2*). We just recall that in the laser-induced fluorescence experiments, heated nickel vapor reacts with CH_3Cl to produce NiCl molecules which interact with a cw tunable laser beam. The resultant fluorescence is dispersed with a Jobin–Yvon spectrometer. The Fourier transform spectra were recorded with a Bruker IFS 120 HR spectrometer with emission induced by a 2 450-MHz microwave discharge exciting a continuous flow of heated $NiCl_2$ vapor and He buffer gas in a quartz tube.

III. DESCRIPTION OF THE BANDS

The strong ionicity of halide compounds forces the low-lying molecular electronic configurations to be centered on the 3*d* atomic orbital of the metal atom. In the case of NiCl, as for NiF, the $^2\Sigma^+$, $^2\Pi_i$, and $^2\Delta_i$ states corresponding to the $3d\sigma^{-1}$, $3d\pi^{-1}$, and $3d\delta^{-1}$ electron holes are expected to be low-lying in the energy level diagram. In previous papers (*1, 2*), some of the spin components associated with these three terms have been identified (see Fig. 1 of Ref. *2*).

Laser-induced dispersed fluorescence experiments have been performed. The three already known upper electronic spin–orbit components [24.9]$\,^2\Pi_{1/2}$ ($v = 0$), [24.5]$\,^2\Pi_{3/2}$ ($v = 0$), and [21.9]$\,^2\Delta_{5/2}$ ($v = 0$) were populated using a dye laser and we

0022-2852/01 $35.00

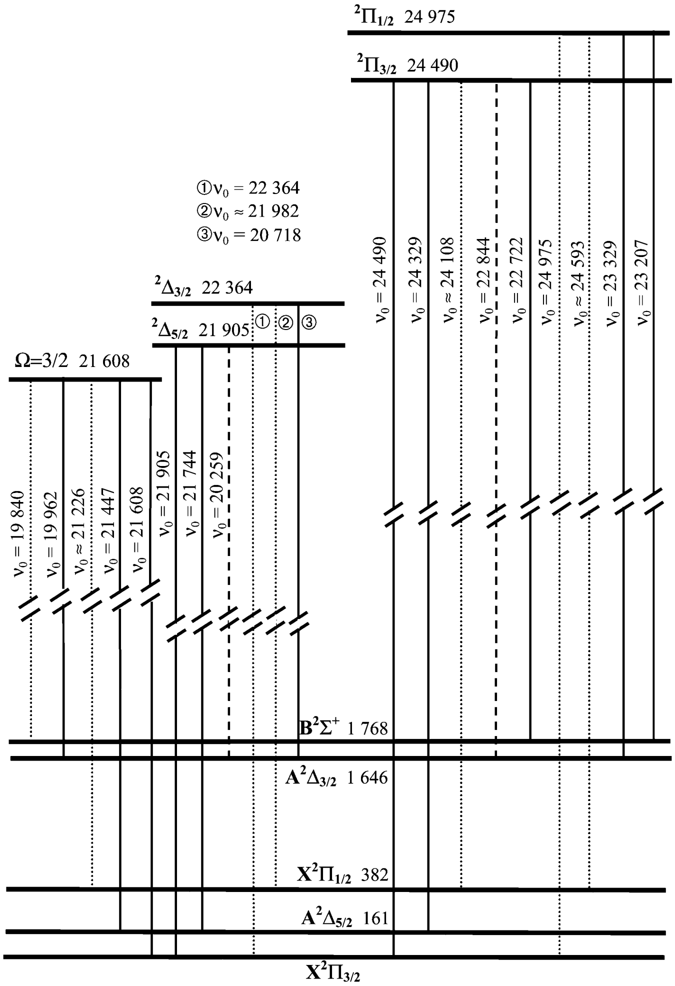

FIG. 1. Energy level diagram of NiCl: Full lines: analyzed allowed transitions. Dashed lines: analyzed forbidden transitions. Dotted lines: observed transitions. All entries are in cm^{-1}.

systematically recorded the induced fluorescence. Beside some 0–1 vibrational bands these experiments led to the identification of five transitions linking two or three of the upper states to two low-lying states located at 1 646 cm^{-1} and 382 cm^{-1} above the $X\,^2\Pi_{3/2}$ state (Fig. 1). The low-resolution data was compared with observations of the bands recorded by Fourier transform spectroscopy.

From these considerations it has been possible to determine that the $\Omega = 3/2$ state located at 1 646 cm^{-1} in the energy level diagram is the $[1.6]\,^2\Delta_{3/2}$ spin–orbit component of the $A\,^2\Delta_i$ state associated with the $[0.16]\,^2\Delta_{5/2}$ sublevel located at 161 cm^{-1}. Because of the correlation between the molecular orbitals and the 3d orbital of Ni^+, it is expected that the spin–orbit splitting (1 485 cm^{-1}) of the $A\,^2\Delta_i$ is about twice the value of the atomic spin–orbit coefficient ($\xi = 603$ cm^{-1}) of the $[3d^9]\,^2D$ ground state of Ni^+ (*6*). Considering the interactions possible between the close-lying $B^2\Sigma^+$, $X\,^2\Pi_i$, and $A\,^2\Delta_i$ states, the agreement between the experimental value (1 485 cm^{-1}) and the theoretical one (1 206 cm^{-1}) is convincing. We also note that this value agrees also with the spin–orbit splitting of the $A\,^2\Delta_i$ state of NiF which is equal to 1 394 cm^{-1}.

It is tempting to use the same kind of arguments for the $\Omega = 1/2$ state located at 382 cm^{-1} above the $X\,^2\Pi_{3/2}$ component of the ground state. The spin–orbit splitting, in the case of a $^2\Pi$ state, must be equal to the value of the spin–orbit coefficient of the ground state of Ni^+. The discrepancy is almost 40% and the identity of the new state must be confirmed by rotational analysis. Note that in the case of NiF, the $X^2\Pi_{1/2}$ state has not been identified but that a so-called $^2\Sigma^+$ state, located 251 cm^{-1} above the ground, has been rotationally analyzed (*7*, *8*).

Regardless of the symmetry attributed to the $\Omega = 1/2$ sublevel located 382 cm^{-1} above the $X\,^2\Pi_{3/2}$ state, we have now a good knowledge of the relative position of the doublet states appearing in the first 2 000 cm^{-1} above the ground state of NiCl. Scanning the laser to the red side of the $[21.9]\,^2\Delta_{5/2}$ $(v = 0)$–$[0.16]$ $A\,^2\Delta_{5/2}$ $(v = 0)$ transition located at 21 744 cm^{-1} (*1*), we observed an intense fluorescence signal when the laser excited a strong R head (21 610 cm^{-1}). A survey scan of the spectral region to lower wavenumbers showed that fluorescence signals were observed at 21 450 cm^{-1}, 21 230 cm^{-1}, 19 967 cm^{-1}, and 19 844 cm^{-1}. It was then easy to conclude that a state located at about 21 608 cm^{-1} in the energy level diagram was populated and that we recorded laser-induced fluorescence down to all the known low-lying states of NiCl. Selection rules do not provide information on the nature of the new upper state because a comparison of intensities of the bands recorded by Fourier transform spectroscopy is not convincing. Rotational analysis of three transitions sharing this new upper state allowed us to identify it as a $\Omega = 3/2$ component. In the separate set of experiments, the fluorescence signals, selection rules and the patterns of emission did allow us to ascertain that the upper state of three transitions located at 22 370 cm^{-1}, 21 987 cm^{-1}, and 20 723 cm^{-1} is the $[22.3]\,^2\Delta_{3/2}$ spin–orbit component associated with the known $[21.9]\,^2\Delta_{5/2}$ state.

IV. ROTATIONAL ANALYSIS OF THE BANDS

(a) Introduction

A characteristic of the emission spectrum of NiCl recorded in the spectral region of 20 000–25 000 cm^{-1} is that only two bands $[21.9]\,^2\Delta_{5/2}$ $(v = 0)$–$[0.16]$ $A\,^2\Delta_{5/2}$ $(v = 0)$ and $[21.9]\,^2\Delta_{5/2}$ $(v = 0)$–$X\,^2\Pi_{3/2}$ $(v = 0)$ have a very good signal-to-noise ratio (see Fig. 1 of Ref. *1*), although the other bands also display rotational structure. As a consequence analyses of the bands described hereafter have been carried out simultaneously to allow the comparison of combination differences of common states. In addition, Professor Tanimoto at Shizuoka University (*9*, *10*) provided very accurate rotational parameters derived from microwave experiments for the $X\,^2\Pi_{3/2}$ $(v = 0)$ and the

[0.16] $^2\Delta_{5/2}$ ($v = 0$) substates. These values have been used as fixed parameters in the fits.

(b) The [24.9] $^2\Pi_{1/2}$–[1.6] $A\,^2\Delta_{3/2}$ and [24.5] $^2\Pi_{3/2}$–[1.6] $A\,^2\Delta_{3/2}$ Transitions

Up to now, four transitions from the spin–orbit components of the upper $^2\Pi_i$ state have been studied, and two of them allowed us to determine the rotational and fine structure parameters of the [1.7]$B\,^2\Sigma^+$ ($v = 0$) state (*2*). Our new data shows that the two components of the upper $^2\Pi_i$ state are also linked to the [1.6]$A\,^2\Delta_{3/2}$ substate. Qualitative observation of the emission spectrum shows that the [24.9] $^2\Pi_{1/2}$–[1.6]$A\,^2\Delta_{3/2}$ transition is an allowed transition (with Q branches), while the [24.5] $^2\Pi_{3/2}$–[1.6]$A\,^2\Delta_{3/2}$ is a weak forbidden transition (without a Q branch). The wavenumbers of the experimental lines of these two new transitions have been included in a fit along with the four previously studied transitions (*2*). In the fitting procedure, the same matrix used previously (*2*) for the upper $^2\Pi_i$ state was employed, while a polynomial expression (*1*) was used to describe the two widely separated components of the $A^2\Delta_i$ state. Experimental lines are listed in Table 1 and the derived parameters in Table 2. We note that it has been possible to determine the Λ-doubling parameter q in the upper $^2\Pi_i$ state in this study. In the previous analysis (*2*), the excited $^2\Pi_{1/2}$ was only connected to the [1.7]$B^2\Sigma^+$ ($v = 0$) state. However, in this transition only four of the six expected branches were identified, hence there was a strong correlation between the parameter q and the spin-rotation parameter γ_D of the [1.7]$B\,^2\Sigma^+$ state. In the present fit, the forbidden [24.5] $^2\Pi_{3/2}$–[1.6]$A\,^2\Delta_{3/2}$ transition gave a good value for the effective Λ-doubling parameter p_D of the [1.6]$A\,^2\Delta_{3/2}$ lower state. The variance of the fit was significantly improved by the presence of the parameter q in the upper $^2\Pi_{1/2}$ state.

(c) The [21.9] $^2\Delta_{5/2}$ ($v = 0$)–[1.6] $A\,^2\Delta_{3/2}$ ($v = 0$) Transition

This transition is the only forbidden one that we found involving the upper [21.9] $^2\Delta_{5/2}$ state. The presence of Q branches is characteristic of a $\Delta\Omega \neq 0$ transition as expected. In a first step we calculated the wavenumbers for the rotational lines based on the parameters determined in the previous section for the [1.6] $A\,^2\Delta_{3/2}$ state and those in Ref. *1* for the [21.9] $^2\Delta_{5/2}$ ($v = 0$) state and we picked out the lines of the six branches in the experimental spectrum recorded by Fourier transform spectroscopy. Then (as for the previous set of bands) the lines were fitted along with the 0–0 bands of the [21.9] $^2\Delta_{5/2}$–[0.16]$A^2\Delta_{5/2}$ and [21.9] $^2\Delta_{5/2}$–$X\,^2\Pi_{3/2}$ transitions (*1*) fixing the parameters for the two lower states to the values determined by Yamazaki *et al.* (*9, 10*).

We found a mistake in Table 3 of Ref. *1*: the lines listed for the Q_{ef} branch of the [21.9] $^2\Delta_{5/2}$ ($v = 0$)–$X\,^2\Pi_{3/2}$ ($v = 0$) are not corrected by the calibration factor. All the entries of this column must be multiplied by the factor 1.000 002 23. This has no consequence for the derived parameters, which were fitted with correct wavenumbers in Ref. *1*.

(d) The [21.6] $\Omega = 3/2$ Electronic State and Linked Transitions

As observed for the [24.5] $^2\Pi_{3/2}$ state, the new [21.6] $\Omega = 3/2$ state is involved in transitions that connect to all the identified components of the low-lying doublet states. The intense [21.6] $\Omega = 3/2$–$X\,^2\Pi_{3/2}$ transition observed at 21 608 cm^{-1} has been directly studied. The J-numbering of the lines was easily determined thanks to the usual combination relationships associated with the good constants available for the ground state (*9*). No fine structure was found in the upper state. Next the weak [21.6]$\Omega = 3/2$–[0.16]$A\ ^2\Delta_{5/2}$ and [21.6] $\Omega = 3/2$–[0.16]A $^2\Delta_{3/2}$ transitions were predicted to make the identification of the experimental lines easy, and finally the lines of the three transitions sharing the upper [21.6] $\Omega = 3/2$ state were fitted by constraining the constants of the $X\,^2\Pi_{3/2}$ and [0.16]$A\,^2\Delta_{5/2}$ states to the values determined from microwave data (*9, 10*). All the lines are listed in Table 1 and the derived parameters in Table 2.

No efforts were made to analyze the very weak [21.6] $\Omega = 3/2$–[1.7]$B\,^2\Sigma^+$ transition (19 840 cm^{-1}) in which the rotational structure was not resolved because of the poor signal-to-noise ratio. In addition, some information about the position of bands involving higher vibrational levels of the studied states is collected in Table 3. From this list of bandhead positions, it is possible to determine approximately the vibrational parameters of the [21.6]$\Omega = 3/2$ state ($\omega_e = 406.1(2)$ cm^{-1}, $\omega_e x_e = 2.6(2)$ cm^{-1}) and the $\Delta G_{1/2}$ value of the [1.6]$A\,^2\Delta_{3/2}$ state ($\Delta G_{1/2} = 429.9(5)$ cm^{-1}).

(e) The [22.3] $^2\Delta_{3/2}$ State and the Linked Transitions

The number of unassigned bands between 20 000 and 25 000 cm^{-1} are now rather few. Most of them are not fully resolved but the bandheads are clearly visible. The correctness of the pattern that we suggest for the low-lying states can be confirmed by identifying new upper states linked to some of the components of the X, A, and B states.

In the course of the work described in the previous section we identified some vibrationally-excited bands, among which is the [21.6]$\Omega = 3/2$ ($v = 2$)–$X^2\Pi_{3/2}$ ($v = 1$) one (21 988 cm^{-1}). In the emission spectrum this band is significantly stronger than the 1–0 band (22 014 cm^{-1}) of the same transition. We suspected that another band overlapped with the 2–1 band. Tuning the laser to this spectral region, we observed two weak fluorescence signals (R-heads) at 20 723 cm^{-1} and 22 370 cm^{-1}. A new upper state is therefore located at about 22 364 cm^{-1}, and this state is involved in three transitions connecting to the [1.6]$A\,^2\Delta_{3/2}$ state (band head observed at 20 723 cm^{-1}), the [0.38]$X\,^2\Pi_{1/2}$ state (band head at 21 988 cm^{-1}, which overlaps

TABLE 1
Observed Lines Positions (in cm^{-1}) of the Studied Transitions of $^{58}Ni^{35}Cl$

[21.6] $\Omega = 3/2$–$X\,^2\Pi_{3/2}$

J	R_{ee}	R_{ff}	P_{ee}	P_{ff}	J	R_{ee}	R_{ff}
8.5			21605.102	21605.102	43.5	21610.210	21610.318
9.5					44.5	21609.916	21610.033
10.5			21604.101	21604.101	45.5	21609.606	21609.734
11.5			21603.573	21603.573	46.5	21609.278	21609.404
12.5			21603.054	21603.054	47.5	21608.944	21609.076
13.5			21602.509	21602.509	48.5	21608.589	21608.737
14.5			21601.957	21601.957	49.5	21608.220	21608.372
15.5			21601.393	21601.393	50.5	21607.838	21608.004
16.5			21600.807	21600.807	51.5	21607.439	21607.612
17.5			21600.204	21600.204	52.5	21607.028	21607.210
18.5			21599.603	21599.603	53.5	21606.600	21606.798
19.5			21598.972	21598.972	54.5	21606.163	21606.383
20.5			21598.324	21598.324	55.5	21605.706	21605.928
21.5			21597.668	21597.668	56.5	21605.237	21605.463
22.5			21597.011	21597.011	57.5	21604.737	21604.992
23.5			21596.329	21596.329	58.5		21604.515
24.5			21595.617	21595.617	59.5	21603.735	21604.009
25.5			21594.925	21594.925	60.5	21603.190	21603.476
26.5			21594.192	21594.192	61.5	21602.647	21602.949
27.5			21593.447	21593.447	62.5	21602.083	21602.398
28.5			21592.679	21592.679	63.5	21601.521	21601.834
29.5					64.5	21600.935	21601.269
30.5	21612.736	21612.736			65.5	21600.334	21600.674
31.5	21612.639	21612.648	21590.351	21590.351	66.5	21599.710	21600.081
32.5	21612.488	21612.537	21589.522	21589.522	67.5	21599.069	21599.464
33.5	21612.362	21612.407	21588.709	21588.709	68.5	21598.402	21598.837
34.5	21612.200	21612.253	21587.852	21587.852	69.5	21597.751	21598.180
35.5	21612.035	21612.109	21587.002	21587.002	70.5	21597.055	21597.524
36.5	21611.861	21611.920	21586.117	21586.155			
37.5	21611.674	21611.745	21585.221	21585.281			
38.5	21611.467	21611.544	21584.325	21584.398			
39.5	21611.242	21611.330	21583.413	21583.485			
40.5	21611.003	21611.098	21582.489	21582.550			
41.5	21610.756	21610.854	21581.547	21581.589			
42.5	21610.492	21610.589	21580.604	21580.672			

[21.6] $\Omega = 3/2$–$A^2\Delta_{5/2}$

J	Q	P	J	Q	P	J	Q	P
13.5	21445.224		33.5	21436.125	21424.455	53.5	21419.522	21400.946
14.5	21444.947		34.5	21435.467	21423.444	54.5	21418.491	21399.575
15.5	21444.668		35.5	21434.804		55.5		21398.204
16.5	21444.343		36.5	21434.122	21421.415	56.5	21416.394	21396.759
17.5	21444.019		37.5	21433.419	21420.370	57.5	21415.315	21395.347
18.5	21443.654	21437.212	38.5	21432.686	21419.279	58.5	21414.207	21393.911
19.5	21443.272	21436.501	39.5	21431.930	21418.189	59.5	21413.104	21392.425
20.5	21442.885	21435.742	40.5	21431.178	21417.091	60.5	21411.947	21390.969
21.5	21442.483	21435.005	41.5	21430.377	21415.950	61.5	21410.801	21389.480
22.5	21442.045	21434.236	42.5	21429.587	21414.809	62.5	21409.631	21387.954
23.5	21441.621	21433.419	43.5	21428.768		63.5	21408.433	21386.410
24.5	21441.171	21432.633	44.5	21427.904	21412.431	64.5	21407.234	21384.845
25.5	21440.675	21431.782	45.5	21427.055	21411.240	65.5	21405.993	
26.5	21440.157	21430.943	46.5	21426.186	21410.024	66.5	21404.754	
27.5	21439.657	21430.049	47.5	21425.294	21408.770	67.5	21403.513	
28.5	21439.104	21429.179	48.5	21424.382	21407.508	68.5	21402.207	
29.5	21438.564	21428.274	49.5	21423.444	21406.228	69.5	21400.910	
30.5	21437.974	21427.350	50.5	21422.477	21404.947	70.5	21399.575	
31.5	21437.367	21426.405	51.5	21421.516	21403.638			
32.5	21436.765	21425.447	52.5	21420.529	21402.287			

TABLE 1—*Continued*

[21.6] $\Omega = 3/2$–$A^2\Delta_{3/2}$

J	R_{ff}	R_{ee}	P_{ff}	P_{ee}	J	R_{ff}	R_{ee}
3.5			19961.455	19961.455	39.5	19964.197	19964.331
4.5			19961.051	19961.051	40.5	19963.916	19964.032
5.5			19960.565	19960.565	41.5	19963.588	19963.734
6.5			19960.151	19960.151	42.5	19963.274	19963.443
7.5			19959.670	19959.670	43.5	19962.926	19963.092
8.5			199 59.199	19959.199	44.5	19962.561	19962.760
9.5			19958.708	19958.708	45.5	19962.189	19962.388
10.5			19958.182	19958.182	46.5	19961.816	19962.013
11.5			19957.643	19957.643	47.5	19961.389	19961.606
12.5			19957.071	19957.071	48.5	19960.956	19961.197
13.5			19956.536	19956.536	49.5	19960.516	19960.787
14.5			19955.963	19955.963	50.5	19960.066	19960.352
15.5			19955.355	19955.355	51.5	19959.585	19959.887
16.5			19954.746	19954.746	52.5	19959.109	19959.445
17.5			19954.122	19954.122	53.5	19958.571	19958.943
18.5			19953.491	19953.491	54.5	19958.071	19958.437
19.5			19952.838	19952.838	55.5	19957.551	19957.933
20.5			19952.152	19952.152	56.5	19957.023	19957.415
21.5			19951.472	19951.472	57.5	19956.427	
22.5					58.5	19955.858	19956.322
23.5			19950.039	19950.039	59.5	19955.270	19955.755
24.5			19949.288	19949.288	60.5	19954.627	19955.166
25.5			19948.545	19948.545	61.5	19954.002	19954.529
26.5	19966.646	19966.646	19947.799	19947.799	62.5	19953.371	19953.972
27.5	19966.509	19966.509	19947.010	19947.010	63.5	19952.691	19953.322
28.5	19966.407	19966.407	19946.196	19946.196	64.5	19952.040	19952.691
29.5	19966.289	19966.310	19945.379	19945.379	65.5	19951.348	19952.040
30.5	19966.149	19966.185			66.5		19951.348
31.5	19966.001	19966.053			67.5	19949.933	
32.5	19965.817	19965.870			68.5	19949.159	19949.992
33.5	19965.633				69.5	19948.424	19949.288
34.5	19965.441	19965.528			70.5	19947.666	19948.545
35.5	19965.219	19965.321			71.5	19946.875	19947.799
36.5	19964.995	19965.091			72.5	19946.092	19947.016
37.5	19964.744	19964.852			73.5		19946.269
38.5	19964.481	19964.596			74.5		19945.509

[21.9]$^2\Delta_{5/2}$–$A^2\Delta_{3/2}$

J	Q_{ef}	Q_{fe}	P_{ff}	P_{ee}	R_{ee}	R_{ff}
12.5	20258.128	20258.128				
13.5	20257.921	20257.921				
14.5	20257.718	20257.718	20252.647	20252.647		
15.5	20257.510	20257.510	20252.034	20252.034		
16.5	20257.262	20257.262				
17.5	20257.004	20257.004	20250.872	20250.872		
18.5	20256.756	20256.756	20250.258	20250.258		
19.5	20256.448	20256.448	20249.644	20249.644		
20.5	20256.175	20256.175	20248.965	20248.965		
21.5	20255.861	20255.861				
22.5	20255.522	20255.560	20247.635	20247.635		
23.5		20255.205	20246.955	20246.984		
24.5		20254.862	20246.263	20246.305		
25.5			20245.571	20245.571		
26.5	20254.075		20244.800	20244.873		
27.5	20253.680	20253.725	20244.074	20244.139		
28.5	20253.260	20253.327	20243.320	20243.362		
29.5	20252.866	20252.912	20242.538	20242.586		
30.5	20252.420	20252.455	20241.774	20241.814	20263.513	
31.5	20251.975	20252.034	20240.937	20241.061	20263.401	

TABLE 1—*Continued*

$[21.9]^2\Delta_{5/2}$–$A^2\Delta_{3/2}$

J	Q_{ef}	Q_{fe}	P_{ff}	P_{ee}	R_{ee}	R_{ff}
32.5	20251.525	20251.582	20240.113	20240.205		20263.201
33.5	20251.024	20251.113	20239.306	20239.368	20263.164	20263.094
34.5	20250.523	20250.625	20238.452	20238.564	20263.052	20262.917
35.5	20250.027	20250.126	20237.634	20237.723		20262.778
36.5	20249.481	20249.602	20236.731	20236.839	20262.690	20262.578
37.5	20248.965	20249.085	20235.852	20236.015		
38.5	20248.413	20248.525	20234.944	20235.086	20262.336	20262.239
39.5			20234.011	20234.203	20262.150	20261.992
40.5	20247.262	20247.430	20233.078	20233.310	20261.918	20261.736
41.5	20246.672	20246.822	20232.182	20232.348	20261.695	20261.518
42.5	20246.046	20246.263			20261.425	20261.258
43.5	20245.438	20245.631			20261.188	20260.997
44.5	20244.800	20245.003			20260.890	20260.714
45.5	20244.139	20244.391			20260.584	20260.346
46.5	20243.465	20243.705			20260.305	20260.030
47.5	20242.815	20243.067			20259.993	20259.691
48.5	20242.117	20242.369				
49.5	20241.413	20241.671			20259.319	20258.984
50.5	20240.654	20240.991			20258.947	20258.598
51.5	20239.920	20240.251				20258.236
52.5	20239.174	20239.529			20258.189	20257.808
53.5	20238.404	20238.759			20257.757	
54.5	20237.634	20238.013			20257.343	20256.966
55.5	20236.839	20237.242				20256.515
56.5	20236.015	20236.472			20256.515	20256.083
57.5					20256.036	20255.623
58.5						20255.116

$[24.9]^2\Pi_{1/2}$–$A^2\Delta_{3/2}$

J	R_{ee}	R_{ff}	P_{ee}	Q_{ef}	P_{ff}	Q_{fe}
8.5						
9.5				23328.479	23325.357	
10.5				23328.301	23324.865	
11.5				23328.120	23324.372	
12.5				23327.955	23323.824	
13.5				23327.712	23323.317	23328.016
14.5			23322.471	23327.508	23322.734	23327.805
15.5			23321.855	23327.235	23322.174	23327.592
16.5			23321.264	23326.992	23321.577	23327.355
17.5				23326.732	23320.961	23327.122
18.5			23320.015	23326.437	23320.361	
19.5			23319.373	23326.133	23319.710	23326.547
20.5			23318.666	23325.819	23319.069	23326.261
21.5			23318.018	23325.472	23318.403	23325.975
22.5			23317.292	23325.143	23317.741	
23.5			23316.632	23324.775	23317.062	23325.286
24.5			23315.899	23324.371	23316.330	23324.962
25.5			23315.146	23323.991	23315.613	23324.575
26.5				23323.585	23314.894	23324.202
27.5				23323.170		23323.784
28.5	23333.063		23312.834	23322.732		23323.376
29.5	23332.957		23312.071	23322.261	23312.581	23322.937
30.5	23332.865		23311.228	23321.803	23311.800	23322.519
31.5	23332.740		23310.433	23321.316		23322.034
32.5	23332.581		23309.592	23320.813	23310.128	23321.578
33.5			23308.711	23320.316	23309.319	23321.076
34.5		23332.865	23307.860	23319.795	23308.444	23320.588
35.5	23332.043	23332.739	23306.987	23319.256	23307.564	23320.080
36.5	23331.867		23306.103	23318.665	23306.692	23319.543

TABLE 1—*Continued*

$[24.9]^2\Pi_{1/2}$–$A^2\Delta_{3/2}$

J	R_{ee}	R_{ff}	P_{ee}	Q_{ef}	P_{ff}	Q_{fe}
37.5	23331.660		23305.145	23318.113	23305.807	23319.006
38.5	23331.410	23332.105	23304.279	23317.510	23304.876	23318.459
39.5	23331.196	23331.864	23303.285	23316.912	23303.935	23317.867
40.5	23330.923	23331.607	23302.375	23316.292	23303.019	23317.292
41.5	23330.637		23301.402	23315.664	23302.026	23316.679
42.5		23331.066	23300.422	23315.023	23301.061	23316.065
43.5	23330.087	23330.753	23299.426		23300.060	23315.455
44.5	23329.748		23298.425	23313.692	23299.050	23314.793
45.5	23329.420	23330.087	23297.371	23313.003	23298.050	
46.5	23329.078	23329.746	23296.332	23312.304	23296.984	23313.462
47.5	23328.709	23329.422	23295.286	23311.586	23295.931	23312.787
48.5	23328.363	23329.028	23294.215	23310.837	23294.879	23312.072
49.5	23327.954	23328.648	23293.179	23310.086		23311.368
50.5	23327.552		23292.033	23309.315	23292.722	23310.647
51.5	23327.121		23290.961	23308.551	23291.596	23309.887
52.5	23326.731		23289.821	23307.756		23309.134
53.5	23326.259		23288.706	23306.934	23289.363	23308.357
54.5	23325.817		23287.554	23306.104	23288.206	23307.570
55.5	23325.320			23305.280		23306.786
56.5	23324.863			23304.420		23305.967
57.5	23324.369			23303.553		23305.145
58.5	23323.828			23302.683		23304.280
59.5	23323.316			23301.771		23303.444
60.5	23322.797			23300.854		
61.5	23322.225			23299.932		23301.709
62.5	23321.683			23298.996		23300.813
63.5	23321.076			23298.050		23299.914
64.5	23320.468			23297.076		23298.994
65.5	23319.900			23296.091		23298.050
66.5	23319.256			23295.079		23297.088
67.5	23318.623			23294.068		
68.5				23293.042		
69.5	23317.292			23292.025		
70.5	23316.632			23290.962		
71.5				23289.891		
72.5				23288.811		

$[24.5]^2\Pi_{3/2}$–$A^2\Delta_{3/2}$

J	R_{ee}	R_{ff}	P_{ee}	P_{ff}
18.5			22835.299	22835.299
19.5				
20.5			22834.000	22834.000
21.5			22833.330	22833.330
22.5				22832.622
23.5			22831.980	22831.939
24.5			22831.256	22831.205
25.5				22830.500
26.5			22829.802	22829.735
27.5				22828.979
28.5			22828.258	22828.198
29.5	22848.412		22827.455	22827.417
30.5	22848.319	22848.215	22826.683	22826.607
31.5	22848.215	22848.107	22825.873	22825.784
32.5	22848.072			22824.930
33.5	22847.922	22847.827	22824.187	
34.5	22847.757	22847.643	22823.307	22823.250
35.5	22847.583	22847.449	22822.453	22822.361

TABLE 1—*Continued*

		$[24.5]^2\Pi_{3/2}$–$A^2\Delta_{3/2}$		
J	R_{ee}	R_{ff}	P_{ee}	P_{ff}
36.5	22847.395	22847.284	22821.567	22821.459
37.5	22847.195	22847.084		
38.5	22846.947		22819.750	22819.642
39.5	22846.757	22846.601	22818.852	22818.702
40.5	22846.474	22846.328		22817.727
41.5	22846.242	22846.052	22816.940	22816.743
42.5	22845.957	22845.779	22815.993	
43.5	22845.658	22845.483	22814.974	
44.5	22845.369	22845.153		
45.5	22845.052	22844.829		
46.5	22844.724	22844.445		
47.5	22844.372	22844.112		
48.5	22844.004	22843.730		
49.5	22843.622	22843.333		
50.5	22843.248	22842.924		
51.5	22842.822	22842.514		
52.5	22842.441	22842.047		
53.5		22841.612		
54.5	22841.526	22841.152		
55.5	22841.101	22840.669		
56.5	22840.615	22840.164		
57.5	22840.116	22839.631		
58.5	22839.631	22839.145		
59.5	22839.103	22838.576		
60.5	22838.576	22838.024		
61.5	22838.024	22837.464		
62.5	22837.465	22836.874		
63.5	22836.922	22836.267		
64.5	22836.340	22835.689		
65.5	22835.766	22835.048		
66.5	22835.149			
67.5	22834.505			
68.5	22833.879			
69.5	22833.225			

with the [21.6] $\Omega = 3/2$ ($v = 2$)–$X\,^2\Pi_{3/2}$ ($v = 1$) band) and the $X\,^2\Pi_{3/2}$ state (bandhead at 22 370 cm^{-1}). In addition, weak fluorescence involving the $[0.16]A\,^2\Delta_{5/2}$ state was observed at 22 201 cm^{-1}, but efforts made to observe a transition to the $[1.7]B\,^2\Sigma^+$ state remained unsuccessful.

A rotational analysis of the band located at 20 723 cm^{-1} was partially successful thanks to the good knowledge of the B rotational constant of the $[1.6]A\,^2\Delta_{3/2}$ state (Table 2). Unfortunately it has not been possible to determine any fine structure parameter because of the lack of high J-value rotational lines. The constants of the $X\,^2\Pi_{3/2}$ state are very well known (*1, 9*), so a simulated set of lines of the R-branch located at 22 364 cm^{-1} reproduced the position of the head with an uncertainty of 0.2 cm^{-1}. This new state is located at $T_0 = 22\,364.4$ cm^{-1}, i.e., 459.2 cm^{-1} above the [21.9] $^2\Delta_{5/2}$ state. Four arguments can be given to suggest that this new state is the $^2\Delta_{3/2}$ spin–orbit component of a $^2\Delta_i$ state associated with the [21.9] $^2\Delta_{5/2}$ state. *First* the rotational constants are rather similar (Table 2); *second* this state is not linked to the $[1.7]B\,^2\Sigma^+$ state; *third* there are no Q-branches in the $\Delta\Omega = 0$ transitions $[21.3]\,^2\Delta_{3/2}$–$[1.6]A\,^2\Delta_{3/2}$ (20 718 cm^{-1}) and [21.3] $^2\Delta_{3/2}$–$X\,^2\Pi_{3/2}$ (21 982 cm^{-1}). Finally, assuming that this new state is a $^2\Delta_{3/2}$ spin–orbit component, the spin–orbit interval is 459 cm^{-1}, in agreement with predictions based on the atomic spin–orbit constant. As for the lower energy states, a strong correlation between the molecular orbitals and the atomic orbitals of Ni^+ can be assumed. In the case of NiF, Carette *et al.* (*6*) located a group of states between 17 500 cm^{-1} and 21 500 cm^{-1} in the energy level diagram, associated with the $[3d^84s]^2D$ electronic state of Ni^+. The spin–orbit coefficient of this state is $\xi = 275$ cm^{-1} (*6*). As noted in Section III, a $^2\Delta_i$ electronic state should exhibit a spin–orbit splitting equal to $2\xi = 550$ cm^{-1}, which is in agreement with the experimental value (459 cm^{-1}).

V. DISCUSSION AND CONCLUSION

By combining the results collected from two experimental methods has made it possible to draw an energy level diagram

TABLE 2
Molecular Constants (in cm^{-1}) for the Electronic States Involved in the Studied Transitions of ^{58}Ni^{35}Cl (All Uncertainties are 1σ)

State	T_0	A_0	B_0	$D_0 \times 10^7$	p_0	$q_0 \times 10^5$	γ_0	$\gamma_D \times 10^7$
$[24.9]^2\Pi_{1/2}$			0.174720(10)					
	24732.865(2)	−484.542(2)		1.287(11)	−0.02006(7)	6.01(10)		
$[24.5]^2\Pi_{3/2}$			0.174870(10)					
$[22.3]^2\Delta_{3/2}$	22364.432^b		0.17550^b	1.208^b				
$[21.9]^2\Delta_{5/2}$	21905.157(2)		0.175125(2)	1.308(3)				
$[21.6]\ \Omega = 3/2$	21608.625(2)		0.174367(4)	1.311(6)				
$[1.7]B^2\Sigma^+$	1768.066(5)		0.179935(10)	1.084(20)			−0.11513(8)	9.69(30)
$[1.6]A^2\Delta_{3/2}$	1645.834(5)		0.182295(4)	1.526(6)		$^a p_D = -0.2405(20)$		

^{a} The [1.6] $A\,^2\Delta_{3/2}$ has been described by a polynomial expression:

$$T = T_0 + B_0 J(J+1) - D_0 J^2(J+1)^2 \pm (1/2) p_D J(J+1)(J+0.5),$$

the + and − refer to the e and f parity levels respectively.
^{b} Estimated constants. See text.

of the low-lying $X\,^2\Pi_i$, $A\,^2\Delta_i$, and $B\,^2\Sigma^+$ states of NiCl (Fig. 1). If we compare this diagram to that of NiF (*3*), we note that in both cases the ground state is a $X\,^2\Pi_{3/2}$ spin–orbit component. The $B\,^2\Sigma^+$ states are located at 1 768 cm^{-1} (NiCl) and at 1 574 cm^{-1} (NiF), the $A\,^2\Delta_{5/2}$ and $A\,^2\Delta_{3/2}$ substates are observed, respectively, at 161 and 1 646 cm^{-1} (NiCl) and 830 and 2 224 cm^{-1} (NiF).

The identification of the $X\,^2\Pi_{1/2}$ spin–orbit component is very puzzling for NiCl as well as for NiF. In the case of NiF a state located 251 cm^{-1} above the ground state has been described as a $^2\Sigma^+$ state (*7*) and a large value ($\gamma = -0.9$ cm^{-1}) of the spin-rotation parameter as been determined. This analysis was possible only with the help of selective excitation using a high-resolution laser. The description of this state has been recently confirmed by Tanimoto *et al.* (*8*). For the two expected $\Omega = 1/2$ low-lying states we found two $^2\Sigma^+$ states rather than a $^2\Sigma^+$ state and a $^2\Pi_{1/2}$ state as expected from the 3*d*-centered atomic orbital model. In Ref. *6* a ligand field theory interpretation of the molecular electronic energy levels of NiF showed that the first $\Omega = 1/2$ state is a mixture of two electronic configurations (67% of $^2\Pi_{1/2}$ state and 33% of $^2\Sigma^+$ state), which could be responsible for the unusual behavior of the so-called $^2\Sigma^+$ state lying at 251 cm^{-1} above the ground state of NiF.

TABLE 3
Bandhead Positions (in cm^{-1})

$v' - v''$	^{58}Ni^{35}Cl
$[21.6]\,\Omega = 3/2$–$X\,^2\Pi_{3/2}$ Transition	
0−0	21 613.1
1−1	21 592.0
1−0	22 013.9
2−1	21 987.7
0−1	21 191.1
1−2	21 173.1
$[21.6]\,\Omega = 3/2$–$A^2\Delta_{3/2}$ Transition	
0−0	19 966.9
1−1	19 942.8
1−0	20 367.8
$[24.5]^2\Pi_{3/2}$–$A^2\Delta_{3/2}$ Transition	
0−0	22 848.6
1−1	22 824.2
$[24.9]^2\Pi_{1/2}$–$A^2\Delta_{3/2}$ Transition	
0−0	23 333.8
1−1	23 307.7
1−0	23 732.6

It turns out that in the case of NiCl the situation is similar. The $[0.38]\,^2\Pi_{1/2}$ state is involved in four intense transitions to the $[21.6]\Omega = 3/2$, the $[22.3]\,^2\Delta_{3/2}$, the $[24.5]\,^2\Pi_{3/2}$, and the $[24.9]\,^2\Pi_{1/2}$ upper states. Up to now, however, attempts to analyze these bands have been unsuccessful despite the fact that the upper states of the transitions are now well known. Such a problem of interpretation also occurs in the analysis of the microwave data (*11*). It seems that, as observed for NiF, the $[0.38]X\,^2\Pi_{1/2}$ spin component is affected by a strong interaction with close-lying states. Despite the congested aspect of the bands we hope to be able to carry out laser experiments as was done successfully in the case of NiF (*7*).

In general, the energy levels of metal halides (MX, X = F, Cl, Br, I) correlate with those of metal hydrides (MH). However, the low-lying electronic energy levels of NiH appear to differ somewhat from those of the nickel halides. For NiH, the ground state is a $^2\Delta$ state and the second and third lowest states are $^2\Sigma^+$ and $^2\Pi$, respectively (*12*), while NiF and NiCl have $^2\Pi$ ground states.

In Section III, it was mentioned that the spin–orbit splitting of the $X\,^2\Pi$ and $A\,^2\Delta$ states did not match very well with the predicted values from the Ni$^+$ atomic value (603 cm^{-1} (*6*)). Field and his co-workers (*12*) pointed out that the low-lying electronic states of NiH severely interact, resulting in large energy level shifts. This complex interaction consists of the spin–orbit interaction due to the 3*d*-electron hole on the Ni^+ atom, rotation–electronic interaction because of the large molecular rotational constant, and accidental perturbations arising when vibrational energy level separations in the $X\,^2\Pi$ and $A\,^2\Delta$, and $B\,^2\Sigma^+$ states happen to match the electronic term values of the $A\,^2\Delta$ and $B\,^2\Sigma^+$ states. The same interaction scheme should be considered for NiF and NiCl. However, the rotation-electronic and vibrational interactions from the "supermultiplet" model (*12*) are negligible for the heavier NiF and NiCl. Thus, the spin–orbit intervals in the $X\,^2\Pi$ and $A\,^2\Delta$ states are strongly affected by off-diagonal spin–orbit interactions among low-lying states: $X\,^2\Pi_{3/2}$ shifts $A\,^2\Delta_{3/2}$ up and $X\,^2\Pi_{1/2}$ is lowered by $B\,^2\Sigma^+$. This is consistent with the fact that the effective molecular spin–orbit coupling constant of the $X\,^2\Pi$ state ($|A_0| \sim 382$ cm^{-1}) is reduced, but that of $A\,^2\Delta(|A_0| \sim 742$ cm^{-1}) state is larger than the prediction ($|A_0| \sim 603$ cm^{-1}) from the Ni^+ atom.

One remaining problem is the presence of a sixth low-lying state located at about 1 385 cm^{-1} on the energy level diagram. This state is involved in an intense transition located at 20 225 cm^{-1} which can be seen in emission when the laser line populates the $[21.6]\Omega = 3/2$ state. Similarly a weak fluorescence is observed at 20 250 cm^{-1}, when the laser populates the $[21.9]\,^2\Delta_{5/2}$ state. We suspect that this new low-lying state to be a component of a quartet state. Carette *et al.* (*6*) showed that components of quartet states are theoretically expected in the first 2 000 cm^{-1} above the ground state of NiF. Recently Chen *et al.* (*13*) carried out a molecular beam experiment on NiF. The temperature of the molecular beam is sufficiently low (90 K) that only the two lowest energy spin components are populated. Laser excitation spectra are then free of transitions involving the other low-lying electronic states. We can hope that this experimental technique (applied to NiCl) could help to answer some of the remaining questions about the energy level diagram of NiCl.

ACKNOWLEDGMENTS

We thank Professor M. Tanimoto at Shizuoka University for sharing his unpublished data. This work was supported by the Natural Sciences and Engineering Research Council of Canada (NSERC). The Centre d'Etudes et de Recherches Lasers et Applications is supported by the Ministère Chargé de la Recherche, the Région Nord-Pas de Calais, and the Fond Européen de Développement Economique des Régions.

REFERENCES

1. T. Hirao, C. Dufour, B. Pinchemel, and P. F. Bernath, *J. Mol. Spectrosc.* **202,** 53–58 (2000).
2. A. Poclet, Y. Krouti, T. Hirao, B. Pinchemel, and P. F. Bernath, *J. Mol. Spectrosc.* **204,** 125–132 (2000).
3. C. Dufour, I. Hikmet, and B. Pinchemel, *J. Mol. Spectrosc.* **165,** 398–405 (1994).
4. S. Paddi Reddi and P. Tiruvenganna Rao, *Proc. Phys. Soc. London* **75,** 275–279 (1960).
5. C. Focsa, C. Dufour, and B. Pinchemel, *J. Mol. Spectrosc.* **182,** 65–71 (1997).
6. P. Carette, C. Dufour, and B. Pinchemel, *J. Mol. Spectrosc.* **161,** 323–335 (1993).
7. C. Dufour and B. Pinchemel, *J. Mol. Spectrosc.* **173,** 70–78 (1995).
8. M. Tanimoto, T. Sakamaki, and T. Okabayashi, *J. Mol. Spectrosc.* **207,** 1–4 (2001).
9. E. Yamazaki, T. Okabayashi, and M. Tanimoto, *Astrophys. J. Lett.* **551,** L199–L201 (2001).
10. E. Yamazaki, T. Okabayashi, and M. Tanimoto, *to be published*.
11. M. Tanimoto, *private communication*.
12. J. A. Gray, M. Li, Th. Nelis, and R. W. Field, *J. Chem. Phys.* **95,** 7164–7178 (1991).
13. Y. Chen, J. Jin, C. J. Hu, X. L. Yang, X. X. Ma, and C. X. Chen, *J. Mol. Spectrosc.* **203,** 37–40 (2000).